Optical Soliton Bullets in (2+1)D Nonlinear Bragg Resonant Periodic Geometries

By Tomáš Dohnal and Alejandro B. Aceves

We consider light propagation in a Kerr-nonlinear 2D waveguide with a Bragg grating in the propagation direction and homogeneous in the transverse direction. Using Newton's iteration method we construct both stationary and travelling solitary wave solutions of the corresponding mathematical model, the 2D nonlinear coupled mode equations (2D CME). We call these solutions 2D gap solitons due to their similarity with the gap solitons of 1D CME (fiber grating). Long-time stable evolution preserving the solitary fashion is demonstrated numerically despite the fact that, as we show, for the 2D CME no local constrained minima of the Hamiltonian functional exist. Building on the 1D study of [1], we demonstrate trapping of slow enough 2D gap solitons at localized defects. We explain the mechanism of trapping as resonant transfer of energy from the soliton to one or more nonlinear defect modes. For a special class of defects, we construct a family of nonlinear defect modes by numerically following a bifurcation curve starting at analytically or numerically known linear defect modes. Compared to 1D the dynamics of trapping are harder to fully analyze and the existence of many defect modes for a given defect potential causes that slow solitons store a part of their energy for virtually all of the studied attractive defects.

Address for correspondence: A. B. Aceves, Department of Mathematics and Statistics, University of New Mexico, Albuquerque, NM 87131, USA; e-mail: aceves@math.unm.edu

1. Introduction

Optical media with their refractive index both periodic in space and nonlinear, i.e., dependent on the intensity of the field, offer very promising and useful applications in optical communication and logic devices. The periodicity of the refractive index induces frequency bands. Linear (small amplitude) pulses with frequency inside one of these bands do not propagate—are evanescent. The nonlinearity, on the other hand, if chosen to be "focusing," induces pulses to localize in their support and increase in peak amplitude and therefore counteracts the natural dispersive and diffractive qualities of the medium. By tailoring the shape and intensity of the pulse one can, in principle, achieve a perfect balance between dispersion/diffraction and focusing and thus obtain a solitary wave solution or its special case, a soliton, of the corresponding mathematical model. Such solutions are interesting objects of analysis but become valuable from the application point of view only if they are stable. It is well known that the stability of solitary waves in optical media usually depends on the number of spatial dimensions in the model, i.e., the number of dimensions in which the solution is allowed to disperse/diffract. For a homogeneous medium (no periodicity) with a focusing cubic nonlinearity, where the model is the nonlinear Schrödinger equations (NLS), it is only in 1D that stable solitary wave solutions exist. In higher dimensions solutions either spread (diffract) or focus and become singular in finite time (point blowup) depending on the value of the Hamiltonian functional (for 2D) or on both the value of the Hamiltonian and the L^2 norm of the initial gradient (for nD, $n > 2$) [2]. In the presence of a suitable periodic structure this type of blowup will likely be arrested although the instability of solitary waves toward focusing and diffraction remains.

In this paper we consider a (2D) medium with the cubic focusing (Kerr) nonlinearity and with a Bragg resonant periodic structure in the direction of propagation (z), often referred to as a "*Bragg grating waveguide*" ([3], Section 3.1). In the corresponding 1D structure (the *fiber grating*, Section 2.1) the combination of Bragg grating and nonlinearity allows for the existence of a family of solitary waves, so-called *Bragg grating solitons* (Section 2.2) with velocities whose absolute value lies between 0 and the speed of light in the corresponding homogeneous medium. These solutions are very attractive from the application point of view firstly because of the tunability in speed and secondly for their short formation lengths. Pulses launched in a bare (no grating) fiber converge to solitons after distances of hundreds of meters, whereas in a fiber grating Bragg grating solitons are formed within centimeters [4–6]. We investigate the existence of 2D analogs to the Bragg grating solitons and after constructing several such candidates, we study their interaction with localized defects demonstrating the possibility of their trapping, analogously to the 1D study in [1, 7], (Section 2.3).

In Section 2, we first briefly introduce the fiber Bragg grating, give the governing mathematical model, the 1D coupled mode equations, and present its analytically known gap soliton solutions. Then we summarize the results of [1, 7] on the trapping of 1D gap solitons at localized defects. In Section 3 the geometry of the 2D waveguide grating and the governing equations are presented and the nonexistence of local constrained minima of the Hamiltonian functional is proved. Then, the Newton's iteration construction of 2D gap solitons is described for both the stationary and the moving case. Section 4 presents preliminary results of the study of soliton interaction with localized defects building on the 1D results summarized in Section 2. A class of defects with analytically known linear defect modes is given and corresponding nonlinear defect modes computed numerically. Finally, the possibility of trapping is demonstrated by several numerical simulations.

2. 1D: Fiber grating

2.1. The geometry and the governing equation

In a fiber grating the electric field is confined in both transverse directions (x, y) via the principle of total internal reflection and it propagates along the fiber length (z) (Figure 1). The linear part n_0 of the refractive index is periodic in z and its variation from the average is small. In other words, we have $n_0^2(x, y, z) \approx \bar{n}_0^2(x, y) + 2\varepsilon\bar{n}_0(x, y)\triangle n(z)$, $0 < \varepsilon \ll \bar{n}_0$, where $\bar{n}_0 \approx 1$ is the average and $\triangle n(z) = \kappa_0 \cos(\lambda z)$ is the oscillatory part. For the Bragg resonance condition the period of $\triangle n(z)$ is chosen to be half that of the carrying plane waves $e^{i(k_z z - \omega t)}$ of light, i.e. $\lambda = 2k_z$, so that strong back reflection occurs. The generation of backward propagating plane waves is clear from the following product present in Maxwell's equations

$$\triangle n(z)e^{i(k_z z - \omega t)} = \frac{\kappa_0}{2}(e^{2ik_z z} + e^{-2ik_z z})e^{i(k_z z - \omega t)}$$

$$= \frac{\kappa_0}{2}e^{i(-k_z z - \omega t)} + \text{nonresonant terms}.$$

One can, therefore, write the electric field as a sum of forward and backward propagating plane waves

$$\vec{E} = U(x, y)\left(E_+(Z, T)e^{i(k_z z - \omega t)} + E_-(Z, T)e^{i(-k_z z - \omega t)} + \text{c.c.}\right)\vec{x}, \quad (1)$$
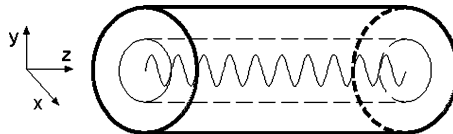
Figure 1. A cartoon of the fiber grating.

where $Z = \varepsilon z$, $T = \varepsilon t$ are "slow" variables, $E_\pm$ are slowly varying envelopes, $\vec{x}$ is the polarization direction, and U is the transverse mode of the fiber. The nonlinearity is chosen to be of Kerr type, i.e., the polarization is $\vec{P} = \chi^{(1)}\vec{E} + \varepsilon\chi^{(3)}|\vec{E}|^2\vec{E}$ and we assume $\max|\triangle n| = \kappa_0 \approx \chi^{(3)}I$, where I is the peak intensity of the electric field. Upon substituting (1) and $\vec{P}$ into Maxwell's equations, multiple scales analysis yields at $\mathcal{O}(1)$ an eigenvalue problem for (ω, U) and at $\mathcal{O}(\varepsilon)$ the 1D coupled mode equations (1D CME) [8] for the envelopes. In dimensionless form 1D CME read

$$
\begin{aligned}
i(\partial_t + \partial_z)E_+ + \kappa E_- + \big(|E_+|^2 + 2|E_-|^2\big)E_+ = 0 \\
i(\partial_t - \partial_z)E_- + \kappa E_+ + \big(|E_-|^2 + 2|E_+|^2\big)E_- = 0,
\end{aligned}
\tag{2}
$$

where κ can be assumed nonnegative without any loss of generality and the independent variables Z, T have been renamed z, t. The system (2) is Hamiltonian, dispersive, nonintegrable via the inverse scattering transform and conservative (conserves $\|E_+\|_2^2 + \|E_-\|_2^2$). The dispersion relation for the modes $e^{i(k_z z - \omega t)}$ is $\omega = \pm\sqrt{k_z^2 + \kappa^2}$, (Figure 2). As the dispersion relation shows, there are no linear (small amplitude) solutions with frequencies in the gap $\omega \in (-\kappa, \kappa)$. Plane waves with frequencies in the gap have imaginary wavenumbers and thus are evanescent.

2.2. Gap solitons in 1D

Existence of solitary wave solutions to the nonlinear problem was first demonstrated numerically in [9] and then given in an explicit form in [10, 11]. These solutions are usually called Bragg grating solitons or gap solitons. They are a family parameterized by a detuning parameter $\delta \in (0, \pi)$ and the velocity $v \in (-1, 1)$, with 1 being the group velocity in the homogeneous medium.

$$
E_\pm = \pm\alpha e^{i\eta}\sqrt{\frac{\kappa}{2}}\sin(\delta)\Delta^{\mp 1}e^{i\sigma}\operatorname{sech}(\theta \mp i\delta/2),
\tag{3}
$$
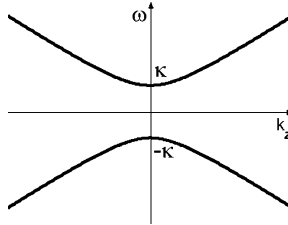
Figure 2. The dispersion relation for (2).

where

$$\alpha = \sqrt{\frac{2(1-v^2)}{3-v^2}}, \qquad \Delta = \left(\frac{1-v}{1+v}\right)^{1/4},$$

$$\theta = \gamma\kappa\sin(\delta)(z-vt), \quad \sigma = \gamma\kappa\cos(\delta)(vz-t),$$

$$\gamma = (1-v^2)^{-1/2}, \qquad e^{i\eta} = \left(-\frac{e^{2\theta}+e^{-i\delta}}{e^{2\theta}+e^{i\delta}}\right)^{\frac{2v}{3-v^2}} = e^{i\frac{4v}{3-v^2}\arctan\left(\frac{e^{2\theta}+\cos(\delta)}{\sin(\delta)}\right)}.$$

The temporal frequency of these solutions (in the travelling wave variables $\zeta = z - vt$, $\tau = t$) is $\omega = \kappa\cos(\delta)\sqrt{1-v^2}$ and thus lies within the linear frequency gap. The frequency of the stationary ($v = 0$) solution lies close to a gap edge for δ close to 0 or π and in the middle of the gap for $\delta = \pi/2$. From the sine factor in formula (3) we see that δ near 0 or π corresponds to small and δ near $\pi/2$ to large amplitude solutions.

It has been shown [12, 13] that gap solitons with $\omega < \omega_c$ for a specific negative ω_c posses an oscillatory instability. Gap solitons with $\omega > \omega_c$ are stable. The stability for $\omega > \omega_c$ is consistent with the fact that for frequencies near the upper edge of the gap the 1D CME are approximated by the focusing 1D NLS that supports stable solitary waves.

2.3. Interaction of 1D gap solitons with localized defects

Here we briefly summarize the results of [1, 7] on the study of the interaction of gap solitons (3) with localized defects. The obtained results include reflection, transmission as well as trapping. Relevant to our 2D model (Section 4) is the authors' derivation of a family of z-localized potentials (defect potentials) $V(z)$, $\kappa(z)$ for which the linear problem

$$\begin{aligned}
i(\partial_t + \partial_z)E_+ + \kappa(z)E_- + V(z)E_+ &= 0 \\
i(\partial_t - \partial_z)E_- + \kappa(z)E_+ + V(z)E_- &= 0
\end{aligned} \tag{4}$$

can be solved explicitly for functions $e^{-i\omega_L t}\vec{\mathcal{E}}(z)$ with $\omega_L \in \mathbb{R}$ and $\vec{\mathcal{E}} = (\mathcal{E}_+, \mathcal{E}_-)$ localized in z. This is done by rewriting (4) in a form equivalent to the Zakharov–Shabat eigenvalue problem for the defocusing NLS. It is shown that the potentials

$$V(z) = \frac{1}{2}\frac{nk^2\Omega\operatorname{sech}^2(kz)}{\Omega^2 + n^2k^2\tanh^2(kz)}, \quad \kappa(z) = \sqrt{\Omega^2 + n^2k^2\tanh^2(kz)} \tag{5}$$

with $\Omega, k \in \mathbb{R}$, and $n \in \mathbb{N}$ support the *linear defect mode*

$$\begin{pmatrix} \mathcal{E}_+ \\ \mathcal{E}_- \end{pmatrix} = \begin{pmatrix} \exp\left(\frac{i}{2}\arctan\frac{nk\tanh(kz)}{\Omega}\right) \\ \mp\operatorname{sign}(\Omega)\exp\left(\frac{-i}{2}\arctan\frac{nk\tanh(kz)}{\Omega}\right) \end{pmatrix}\operatorname{sech}^n(kz) \tag{6}$$

with frequency $\omega_L = \Omega$ as well as $2(n-1)$ other defect modes (hypergeometric functions) with frequencies $\omega_L = \pm\sqrt{\Omega^2 + k^2(2nr - r^2)}$, $\quad r \in \{1, \ldots, n-1\}$. The argument is made, and verified numerically that a gap soliton will be trapped only at such a defect that supports a nonlinear defect mode with frequency equal to that of the gap soliton (*resonance*) and with total power smaller or equal to that of the soliton (*energetic accessibility*). Otherwise the energy stored by the soliton will be reflected and/or transmitted ([1], p. 1642).

3. 2D: *x*-Homogeneous waveguide grating

3.1. The geometry and governing equations

In a waveguide grating the electric field is confined in only one transverse direction (y), it diffracts in the other transverse direction (x), in which the medium is homogeneous and there is a Bragg grating (Section 2.1) in the propagation direction (z) (Figure 3). Analogous to Section 2.1, under the assumption of a balance among the characteristic length scales of coupling, nonlinearity, and diffraction, which means assuming the following form of the electric field

$$\vec{E} = U(y)\left(E_+(X, Z, T)e^{i(k_z z - \omega t)} + E_-(X, Z, T)e^{i(-k_z z - \omega t)} + \text{c.c.}\right)\vec{x}, \quad (7)$$

with $X = \sqrt{\varepsilon}x$, $Z = \varepsilon z$ and $T = \varepsilon t$, the 2D coupled mode equations (2D CME) [14, 15]

$$\begin{aligned}
i(\partial_t + \partial_z)E_+ + \kappa E_- + \partial_x^2 E_+ + \left(|E_+|^2 + 2|E_-|^2\right)E_+ = 0 \\
i(\partial_t - \partial_z)E_- + \kappa E_+ + \partial_x^2 E_- + \left(|E_-|^2 + 2|E_+|^2\right)E_- = 0
\end{aligned} \qquad (8)$$

for the envelopes $E_\pm(x, z, t)$ are obtained. Once again, the independent variables X, Z, T have been renamed x, z, t. Just like (2) this system is Hamiltonian,
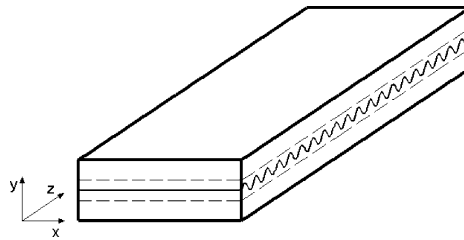
Figure 3. A cartoon of the waveguide grating.

dispersive, nonintegrable, and conservative. The Hamiltonian formulation reads

$$i\partial_t E_\pm = \frac{\delta H}{\delta E_\pm^*}, \quad i\partial_t E_\pm^* = -\frac{\delta H}{\delta E_\pm}$$

with the Hamiltonian functional

$$H = \int_\mathbb{R} \int_\mathbb{R} i\left(E_-^* \partial_z E_- - E_+^* \partial_z E_+\right) - \kappa\left(E_- E_+^* + E_-^* E_+\right)$$

$$+ |\partial_x E_+|^2 + |\partial_x E_-|^2 - \left(\frac{1}{2}|E_+|^4 + 2|E_-|^2|E_+|^2 + \frac{1}{2}|E_-|^4\right) dx\,dz. \quad (9)$$

The dispersion relation for plane waves $e^{i(k_z z + k_x x - \omega t)}$ is $\omega = k_x^2 \pm \sqrt{k_z^2 + \kappa^2}$, i.e., the same as for 1D CME (2) but shifted by k_x^2. The frequency gap for a given k_x is $\omega \in (k_x^2 - \kappa, k_x^2 + \kappa)$.

Existence results for solutions of 2D CME with finite L^2 norm have not been obtained and, in particular, a rigorous proof of absence of point blowup has not been done. It is, however, believed that the z-periodic structure prevents blowup but does not, in general, prevent the instability toward focusing. In [16], a heuristic explanation of this process is made for solutions with frequencies close to the upper edge of the linear frequency gap (from the outside). As shown, in that regime the system is well approximated by a perturbed focusing 2D NLS and hence solutions have a tendency to either collapse or diffract. Because, however, collapse implies broadening of the spectrum in the Fourier space (thus also frequency space) and an eventual overlap with the gap where the NLS approximation is no longer valid, the collapse in the NLS fashion is prevented.

An explanation for the limited amount of rigorous results obtained so far is that most of the tools that helped answer these questions for general NLS fail here. More recently, though, we have made important progress on these issues by a combination of heuristic and semirigorous arguments based on physical, numerical, and asymptotic techniques, which the remainder of the paper shows.

A very important question is whether localized dynamics are always unstable to focusing or diffraction or whether a balance can be achieved. An important result, presented in Theorem 1, shows that the critical points of the Hamiltonian under the constraint of a fixed total power are not minima (this result is also mentioned in [15]). In Hamiltonian systems, minimizers can typically be proved to be stable (in an orbital sense) in the time evolution. For the CME the condition of minimality is, however, only sufficient for linear stability and not necessary [17]. In Section 3.3, we present numerically obtained stationary as well as travelling wave solutions that, despite Theorem 1, appear long lived.

3.2. Bound states and critical points of the Hamiltonian

Let us first define a bound state. A solution of (8) of the form $E_\pm(x, z, t) = e^{-i\omega t}\mathcal{E}_\pm(x, z)$ is a *bound state* if $\omega \in \mathbb{R}$ and $\mathcal{E}_\pm \in L^2(\mathbb{R}^2)$. Suppose that $\mathcal{N} := \int_{\mathbb{R}^2} |\mathcal{E}_+|^2 + |\mathcal{E}_-|^2 dx dz = P > 0$ for such a bound state $E_\pm$, we would then want to know whether

$$(\mathcal{E}_+, \mathcal{E}_-) \text{ is a local minimizer of the } H \text{ (see (9)) within the set } S \qquad (10)$$

of all vector functions $(f_1(x, z), f_2(x, z)) : \mathbb{R}^2 \to \mathbb{C}^2$ satisfying the constraint

$$\int_{\mathbb{R}^2} |f_1|^2 + |f_2|^2 dx dz = P. \qquad (11)$$

THEOREM 1. *Possible bound state solutions of the 2D coupled mode equations* (8) *are not solutions of the minimization problem* (10), (11).

Proof: Assume the existence of a bound state $E_\pm$ with $\mathcal{N} = P$. Consider the following 3-parameter family S_1 of scalings of the assumed (fixed) bound state profile $(\mathcal{E}_+, \mathcal{E}_-)$, i.e., functions $\alpha(\tilde{\mathcal{E}}_+(\tilde{x}, \tilde{z}), \tilde{\mathcal{E}}_-(\tilde{x}, \tilde{z})) := \alpha(\mathcal{E}_+(\frac{x}{\mu}, \frac{z}{\nu}), \mathcal{E}_-(\frac{x}{\mu}, \frac{z}{\nu}))$ with $\alpha, \mu, \nu > 0$. Within S_1 the constraint (11) becomes $\alpha^2 \mu \nu = 1$ and H becomes $H_r = A_1 \alpha^2 \mu - A_2 \alpha^2 \mu \nu + A_3 \frac{\alpha^2 \nu}{\mu} - A_4 \alpha^4 \mu \nu$, where

$$A_1 = i \int_{\mathbb{R}^2} \mathcal{E}_-^* \partial_z \mathcal{E}_- - \mathcal{E}_+^* \partial_z \mathcal{E}_+ \, dx dz, \quad A_2 = \kappa \int_{\mathbb{R}^2} \mathcal{E}_- \mathcal{E}_+^* + \mathcal{E}_-^* \mathcal{E}_+ \, dx dz,$$

$$A_3 = \int_{\mathbb{R}^2} |\partial_x \mathcal{E}_+|^2 + |\partial_x \mathcal{E}_-|^2 \, dx dz,$$

$$A_4 = \frac{1}{2} \int_{\mathbb{R}^2} |\mathcal{E}_+|^4 + 4|\mathcal{E}_+|^2|\mathcal{E}_-|^2 + |\mathcal{E}_-|^4 \, dx dz$$

with $A_1, A_2 \in \mathbb{R}$, $A_3, A_4 > 0$. The constants $A_1, \ldots, A_4$ are scale free. Under the constraint H_r reduces to a function of two variables $H_r(\alpha, \nu) = \frac{A_1}{\nu} + A_3 \alpha^4 \nu^2 - A_4 \alpha^2 - A_2$ and one easily finds that the only critical point with $\alpha, \nu > 0$ is $(\alpha^*, \nu^*) = (\frac{A_1 \sqrt{2A_3}}{A_4^{3/2}}, \frac{A_4^2}{2A_1 A_3})$ and that the discriminant in the second derivative test is $D = -32 \frac{A_1^4 A_3^3}{A_4^5} < 0$, i.e. (α^*, ν^*) is a *saddle*. This shows the lack of the existence of a local constrained minimizer of H. ∎

Note that (α^*, ν^*) must be equal to $(1, 1)$. This is because $(\mathcal{E}_+, \mathcal{E}_-)$, being a solution profile, must be a critical point of the extended Hamiltonian $\hat{H} = H - \omega \int_{\mathbb{R}} \int_{\mathbb{R}} |E_+|^2 + |E_-|^2 \, dx dz$ (with ω fixed at the solution frequency) and therefore also a critical point of its reduced version $\hat{H}_r$. $\hat{H}_r = H_r - \omega$ due to the constraint and thus $(\mathcal{E}_+, \mathcal{E}_-)$ is also a critical point of H_r. Given that the

only critical point of H_r is the saddle (α^*, v^*) and because within S_1 the solution profile $(\mathcal{E}_+, \mathcal{E}_-)$ is represented by $(1, 1)$, we get $(\alpha^*, v^*) = (1, 1)$.

This also yields a necessary condition for a function $e^{-i\omega t}(\mathcal{E}_+(x, z), \mathcal{E}_-(x, z))$ to be a bound state solution of 2D CME. The condition is $\left(\frac{A_1\sqrt{2A_3}}{A_4^{3/2}}, \frac{A_4^2}{2A_1A_3}\right) = (1, 1)$. We have verified that the stationary solutions we find numerically (Section 3.3) do satisfy this condition.

Comparison with 1D: We have checked that performing the same scaling argument on H (as in the proof of Theorem 1) for the *1D* CME one obtains that the reduced Hamiltonian H_r is constant within the family of scalings of an assumed minimizer $(\mathcal{E}_+, \mathcal{E}_-)$ if

$$i \int_{\mathbb{R}} \mathcal{E}_-^* \partial_z \mathcal{E}_- - \mathcal{E}_+^* \partial_z \mathcal{E}_+ \, dz = \frac{1}{2} \int_{\mathbb{R}} |\mathcal{E}_+|^4 + 4|\mathcal{E}_+|^2|\mathcal{E}_-|^2 + |\mathcal{E}_-|^4 \, dz, \quad (12)$$

which is indeed satisfied by the stationary gap solitons, (3) with $v = 0$. If (12) is not satisfied, H_r has either only the trivial minimum ($\alpha = 0$) or only a maximum; in both cases one gets a contradiction with the assumption of the existence of a nontrivial minimizer of H.

3.3. Numerically constructed stationary and moving solutions

Stationary gap solitons: Despite the result of Theorem 1 we have been able to numerically construct solutions that are stationary on long times. To compute the bound state profile $(\mathcal{E}_+, \mathcal{E}_-)$ as well as the frequency ω, we use Newton's iteration method [18] combined with the GMRES iteration [19] for solving the linear system at each Newton step. In fact, this technique has to be used to find just one solution-frequency pair. Afterward, other pairs may be found following the bifurcation curve through the first pair by slowly varying ω and solving for the profiles only. Assuming the bound state solution form $E_\pm(x, z, t) = e^{-i\omega t}\mathcal{E}_\pm(x, z)$ the system (8) becomes an eigenvalue problem for $(\omega, (\mathcal{E}_+, \mathcal{E}_-))$:

$$\omega \vec{\mathcal{E}} = -\left[i\sigma_3\partial_z + \partial_x^2 + \sigma_1\kappa\right]\vec{\mathcal{E}} - N(\vec{\mathcal{E}}, \vec{\mathcal{E}}^*)\vec{\mathcal{E}}, \quad (13)$$

where we have adopted the vector notation with $\vec{\mathcal{E}} = (\mathcal{E}_+, \mathcal{E}_-)^T$, the Pauli matrices $\sigma_1 = \begin{pmatrix} 0 & 1 \\ 1 & 0 \end{pmatrix}$, $\sigma_3 = \begin{pmatrix} 1 & 0 \\ 0 & -1 \end{pmatrix}$, and $N(\vec{\mathcal{E}}, \vec{\mathcal{E}}^*) = \begin{pmatrix} |\mathcal{E}_+|^2+2|\mathcal{E}_-|^2 & 0 \\ 0 & |\mathcal{E}_-|^2+2|\mathcal{E}_+|^2 \end{pmatrix}$.

This system can be solved as a nonlinear system of equations for ω and $(\mathcal{E}_+, \mathcal{E}_-)$ simultaneously if an extra condition is imposed, for example, on the amplitude of $|\mathcal{E}_+|$ or on the total power $\mathcal{N} := \|\mathcal{E}_+\|_2^2 + \|\mathcal{E}_-\|_2^2$. We choose the latter one; given a number $P > 0$ we solve (13) together with the constraint

$$\mathcal{N} = P \quad (14)$$

for ω and $(\mathcal{E}_+, \mathcal{E}_-)$ via Newton's iteration. For its convergence it is crucial to choose an initial guess $(\omega^{(0)}, (\mathcal{E}_+^{(0)}, \mathcal{E}_-^{(0)}))$ close enough to the solution. One

possible initial guess is $(\omega^{(0)}, (\mathcal{F}_+(z)G(x), \mathcal{F}_-(z)G(x)))$, where $e^{-i\omega^{(0)}t}(\mathcal{F}_+, \mathcal{F}_-)^T$ is a stationary 1D gap soliton ((3) with $v = 0$) and G is a suitable x-dependent localized profile. Note that such a separable waveform will most likely not be an exact profile of a bound state solution. To determine a suitable G we substitute $E_\pm^{(0)}(x, z, t) = \mathcal{F}_\pm(z)G(x)e^{-i\omega^{(0)}t}$ into (8), multiply the first/second equation by $\mathcal{F}_\pm^*$, respectively, integrate in $\theta = \gamma\kappa\sin(\delta)z$, and divide by $\int |\mathcal{F}_\pm|^2 \, d\theta$. Given that for $v = 0$ one has $\mathcal{F}_- = -\mathcal{F}_+^*$, we get a single equation for G:

$$G'' - bG + bG^3 = 0 \tag{15}$$

with $b = 3\frac{\int_\mathbb{R} |\mathcal{F}_+|^4 d\theta}{\int_\mathbb{R} |\mathcal{F}_+|^2 d\theta} = -i\frac{\int_\mathbb{R} \mathcal{F}_+^*(\partial_t\mathcal{F}_+ + \partial_z\mathcal{F}_+)d\theta}{\int_\mathbb{R} |\mathcal{F}_+|^2 d\theta} + \kappa\frac{\int_\mathbb{R} \mathcal{F}_+^{*2} d\theta}{\int_\mathbb{R} |\mathcal{F}_+|^2 d\theta}$. b can be calculated exactly, $b = 2\frac{\kappa}{\delta}(\sin(\delta) - \delta\cos(\delta))$. And because $b > 0$ for $0 < \delta \le \pi$, the localized solution of (15) is $G(x) = \sqrt{2}\text{sech}(\sqrt{b}x)$. Now, $(\omega^{(0)}, (\mathcal{F}_+G, \mathcal{F}_-G))$ is used as the initial guess in solving the nonlinear system (13) and (14). Because the initial guess satisfies the symmetry $\mathcal{F}_- = -\mathcal{F}_+^*$, we enforce this symmetry on our solutions $\mathcal{E}_\pm$. This reduces the size of the system by a half. We also assume odd/even symmetries in x and z as satisfied by the initial guess with a final reduction to about one-eighth of the original size. We note that the symmetry $\mathcal{E}_- = -\mathcal{E}_+^*$ is in contrast with stationary solutions found in [15], which satisfy $\mathcal{E}_- = \mathcal{E}_+^*$. Unfortunately, their evolution was not checked numerically.

In solving (13) and (14) we only succeed to obtain convergence of Newton's iteration for gap solitons with frequencies near the upper edge of the linear frequency gap. In the case $\kappa = 1$ with the trivial x-phase ($k_x = 0$), where the gap is $(-1, 1)$, the convergent iterations yield $0.85 < \omega < 0.99$. The reason for the convergence failure for $\omega < 0.85$ remains to be determined. Solutions with $0.85 < \omega < 0.9$ have significant oscillations in the spatial profiles and these increase as ω gets closer to 0.85. Gap solitons with frequency close to the upper edge are relatively wide and also small in amplitude; they are, nevertheless, truly nonlinear states.

Figure 4 shows the stationary 2D gap soliton with $\omega \approx 0.9595$. Both the profile and evolution plots of the modulus (down the middle of the x-width) as well as of the amplitude, total power, and frequency[1] are given. The slight decrease in power and amplitude in the PDE evolution through our code is attributed to the use of a Fourier filter (Appendix A).

Moving gap solitons: Unfortunately, similar to 1D, neither the Lorentzian nor Galilean transformation can be applied to stationary solutions of 2D CME to produce moving ones. We, therefore, construct moving solitons numerically.

---

[1]We measure temporal frequency of stationary bound states via the formula $\omega_\pm = -\frac{\Im(\int E_\pm^* \partial_t E_\pm \, dx \, dz)}{\int |E_\pm|^2 \, dx \, dz}$, where $\omega_+ = \omega_-$ for a stationary bound state solution.
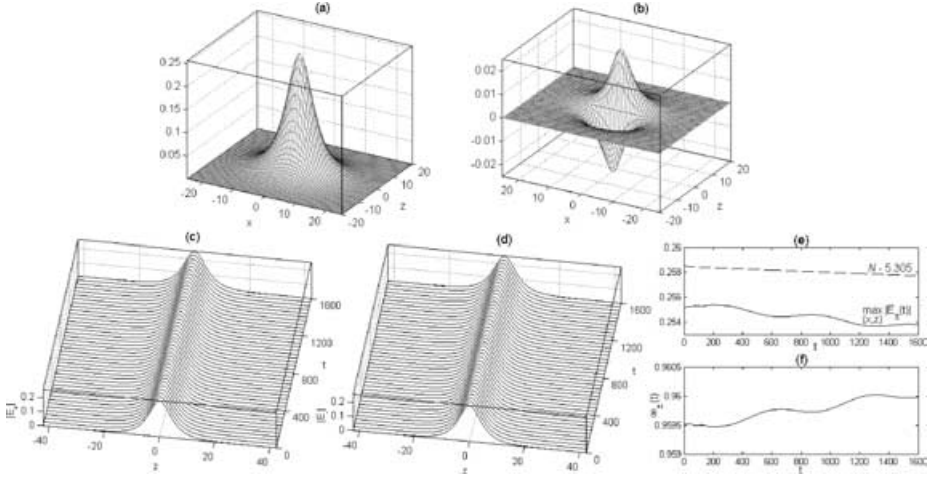
Figure 4. Stationary 2D gap soliton with $\omega \approx 0.9595$ obtained via Newton's iteration ($\kappa = 1$); (a) $\Re(\mathcal{E}_+(x, z)) = -\Re(\mathcal{E}_-(x, z))$, (b) $\Im(\mathcal{E}_+(x, z)) = \Im(\mathcal{E}_-(x, z))$, (c) $|E_+(0, z, t)|$, (d) $E_-(0, z, t)|$, (e) full line: evolution of peak amplitude ($|E_+| = |E_-|$) and dashed line: total power minus a constant, (f) frequency evolution ($\omega_+ = \omega_-$).

A natural ansatz for gap solitons with a nonzero z-speed v is $e^{-i\omega\tau}\mathcal{E}_\pm(x, \zeta)$, where $\zeta = z - vt$, $\tau = t$, $|v| < 1$. For this ansatz 2D CME read

$$\omega\mathcal{E}_+ + i(1-v)\partial_\zeta\mathcal{E}_+ + \kappa\mathcal{E}_- + \partial_x^2\mathcal{E}_+ + \left(|\mathcal{E}_+|^2 + 2|\mathcal{E}_-|^2\right)\mathcal{E}_+ = 0$$
$$\omega\mathcal{E}_- - i(1+v)\partial_\zeta\mathcal{E}_- + \kappa\mathcal{E}_+ + \partial_x^2\mathcal{E}_- + \left(|\mathcal{E}_-|^2 + 2|\mathcal{E}_+|^2\right)\mathcal{E}_- = 0. \tag{16}$$

Once again, we use Newton's iteration to solve (16) for a given v. Unlike for (13) we fix ω and solve only for $(\mathcal{E}_+, \mathcal{E}_-)$. This is for the linear system at each Newton's iteration to be banded, which allows for a more efficient computational treatment. If both v and ω are to be fixed, one is required to know the relation $\omega(v)$. For the 1D gap solitons (3) this relation is $\omega(v) = \omega_0\sqrt{1 - v^2}$, where ω_0 is the frequency of the stationary soliton. Using this relation in (16) leads to a successful convergence, which suggests its validity (for this particular family of gap solitons) also in 2D. We find the solutions of (16) by following the bifurcation curve parameterized by v and starting at $v = 0$. The initial guess for an iteration at $v = n\tilde{\varepsilon}, n \in \mathbb{N}, n < 1/\tilde{\varepsilon}$ is the final iterate at $v = (n-1)\tilde{\varepsilon}$ scaled to satisfy $\frac{\max_{(x,z)} |\mathcal{E}_+|}{\max_{(x,z)} |\mathcal{E}_-|} = \sqrt{\frac{1+v}{1-v}}$. $\tilde{\varepsilon}$ is a small step in the velocity and the particular ratio of amplitudes of the initial guess is chosen based on previous PDE trial runs of various initial conditions, which showed that, remarkably, all moving solutions found (solitary waves, breathers, or diffracting solutions) satisfy this relation. Note that this relation also holds for the 1D gap solitons (3).
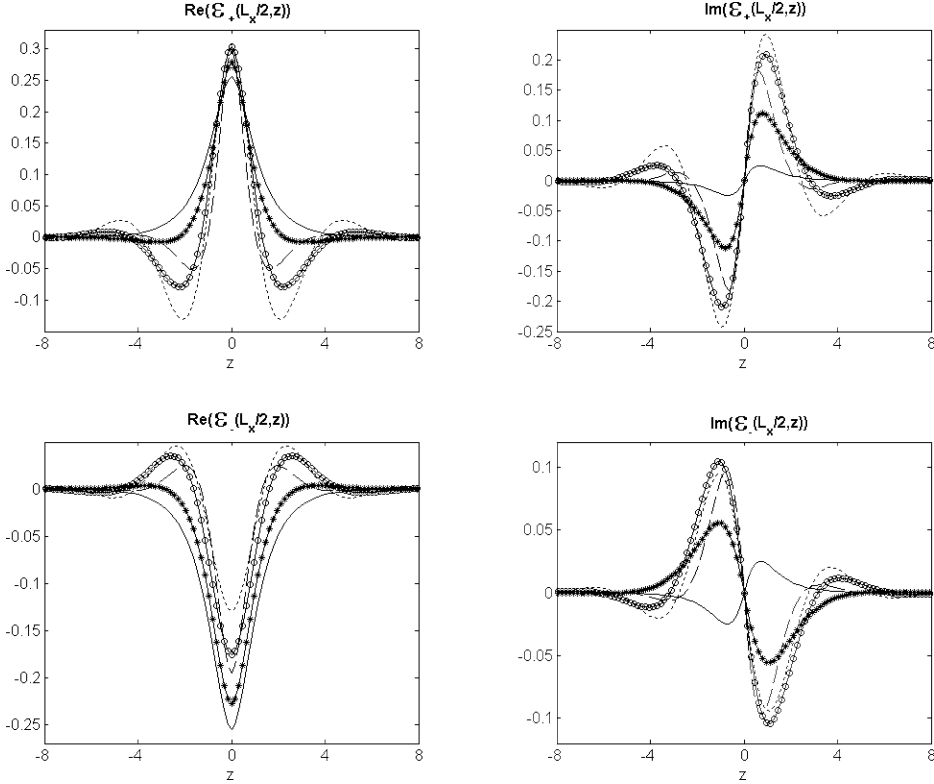
Figure 5. z-profiles of moving solitons for $(\kappa, \omega_0) = (1, 0.9595)$; full line $v = 0$, ($*$) $v = 0.2$, dashed line $v = 0.4$, ($\circ$) $v = 0.6$, dotted line $v = 0.8$.

We use the banded linear solver DGBSV of the LAPACK library for solving the linear system at each Newton step. Figure 5 shows the z-profiles of solitons with various velocities corresponding to $\omega_0 = 0.9595$. The x-profile remains very similar throughout the range of v (for $v = 0$; Figure 4). Also, as Figure 5 shows, profiles of the moving solitons are symmetric in the z directions ($\Re(\mathcal{E}_\pm)$ even and $\Im(\mathcal{E}_\pm)$ odd). This is because the first initial guess (the stationary soliton) has these symmetries and Newton's iteration preserves them. 1D gap solitons (3), on the other hand, satisfy these symmetries only for $v = 0$. Possibly, z-symmetric moving pulses of 1D CME also exist.

Figure 6 shows the propagation of a 2D gap soliton with $v = 0.2$. Long-time evolution exhibits slow weak breathing that demonstrates an instability of the found solution. The subplot (e) shows the validity of the above mentioned relation $\frac{\max_{(x,z)} |\mathcal{E}_+|}{\max_{(x,z)} |\mathcal{E}_-|} = \sqrt{\frac{1+v}{1-v}}$ between the ratio of amplitudes and the velocity.
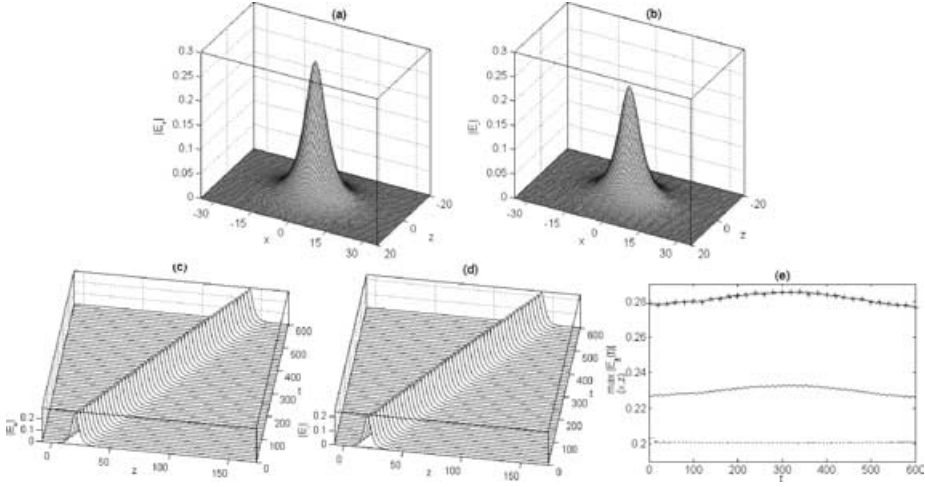
Figure 6. The moving 2D gap soliton with $v = 0.2$, $\omega_0 \approx 0.9595$ obtained via Newton's iteration ($\kappa = 1$); (a) $|E_+(x, z, 0)|$, (b) $|E_-(x, z, 0)|$, (c) $|E_+(0, z, t)|$, (d) $|E_-(0, z, t)|$, (e) peak amplitude evolution: (+) $a_+ := \max_{(x,z)}|E_+|$, full line: $a_- := \max_{(x,z)}|E_-|$, dotted line: $(a_+^2/a_-^2 - 1)/(a_+^2/a_-^2 + 1) \approx v$.

Solutions with an arbitrary nonzero x-component of the velocity can be easily generated by imposing a nontrivial x-phase, i.e., multiplying the above solution profiles by $e^{ik_x x}$, $k_x \in \mathbb{R}$. We, however, concentrate on solutions travelling parallel to the z-axis ($k_x = 0$).

4. Interaction of 2D gap solitons with defects

Analogously to the idea of [1], we study the possibility of trapping 2D gap solitons due to the presence of a localized deterministic defect. Just like in the 1D case of [1] we base our predictions about the nature of interactions on the principle of resonant energy transfer and energy conservation (see end of Section 2.3). In Section 4.1, 4.2, we construct defects and a family of corresponding defect modes and in Section 4.3 we present results of our numerical simulations of soliton–defect interactions.

4.1. Linear defect modes

We first select suitable defect potentials that, if added to the linear 2D CME (Equation (8) without the nonlinear terms) give a system that can be solved exactly for the ansatz $\vec{E}(x, z, t) = e^{-i\omega_L t}\vec{\mathcal{E}}(x, z)$ with $\omega_L \in \mathbb{R}$ and $\vec{\mathcal{E}} = (\mathcal{E}_+, \mathcal{E}_-)^T$ localized. We call $\vec{\mathcal{E}}$ a *linear defect mode*. Ideally, the defect should be represented by some (qualitatively) radially symmetric potentials
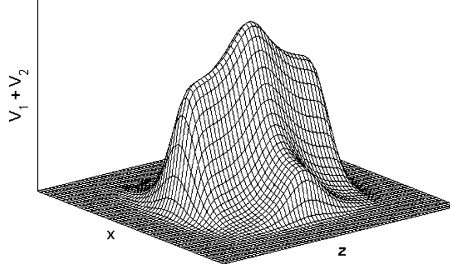
Figure 7.   Example of the defect potential $V_1(x) + V_2(z)$ after support truncation.

$V(x, z), \kappa(x, z)$ centered at (x_0, z_0). Solutions of the linear 2D CME with such V are not known and, hence, we propose the form $V(x, z) = V_1(x) + V_2(z), \kappa = \kappa(z)$, where V_1 and V_2 are smooth and decay to 0 sufficiently fast as $|x - x_0|$ and $|z - z_0|$ grow, respectively, and κ is smooth and similarly approaches a constant value $\kappa_\infty > 0$ (i.e., the coupling coefficient away from the defect) as $|z - z_0|$ grows. Then, for some special choices of $V_{1,2}$ and κ the system

$$\left[\omega + i\sigma_3\partial_z + \partial_x^2 + \sigma_1\kappa(z) + V_1(x) + V_2(z)\right]\vec{\mathcal{E}} = 0 \qquad (17)$$

can be solved exactly via the separation of variables. In Equation (17), ∂_t was replaced with ω to account for the assumed ansatz. Clearly, neither κ nor $V_1 + V_2$ are localized in 2D. This can be fixed by smoothly truncating the support of $V_1(x)$ in the z-direction and of $V_2(z)$ and $\kappa_\infty - \kappa(z)$ in the x-direction at such a distance that the exact solution $E_\pm$ is affected negligibly (see Figure 7 for a schematic of $V_1(x) + V_2(z)$ treated in this way).

Assuming the separation of variables $\mathcal{E}_\pm = F_\pm(z)G(x)$ the system (17) becomes

$$\left[\omega_L - \lambda + i\sigma_3\partial_z + \partial_x^2 + \sigma_1\kappa(z) + V_2(z)\right]\vec{F} = 0, \qquad (18a)$$

$$G'' + (V_1(x) + \lambda)G = 0, \qquad (18b)$$

with $\vec{F} = (F_+, F_-)^T$ and the constant λ being the separation constant. Upon choosing

$$V_1(x) = 2\beta^2\text{sech}^2(\beta x), \quad \beta \in \mathbb{R}, \qquad (19)$$

Equation (18b) with zero decay boundary conditions has a unique eigenfunction $G = \text{sech}(\beta x)$ with $\lambda = -\beta^2$. The problem now reduces to solving (18a) with $\lambda = -\beta^2$. The case $\lambda = 0$ was analyzed in detail in [1, 7] and the results are summarized in Section 2.3. Generalization to $\lambda \neq 0, \lambda \in \mathbb{R}$ only requires a

shift in the frequency $\omega_L \rightsquigarrow \omega_L + \lambda$. In summary, for $V_1(x) = 2\beta^2 \mathrm{sech}^2(\beta x)$ and $V_2(z)$, $\kappa(z)$ given in (5) Equation (17) has the linear defect mode

$$\begin{pmatrix} \mathcal{E}_+ \\ \mathcal{E}_- \end{pmatrix} = \begin{pmatrix} \exp\left(\frac{i}{2}\arctan\frac{nk\tanh(kz)}{\Omega}\right) \\ \mp\mathrm{sign}(\Omega)\exp\left(\frac{-i}{2}\arctan\frac{nk\tanh(kz)}{\Omega}\right) \end{pmatrix} \mathrm{sech}^n(kz)\mathrm{sech}(\beta x), \quad (20)$$

with frequency $\omega_L = \Omega - \beta^2$. The other $2(n-1)$ linear defect modes $F_\pm(z)G(x)$, with $F_\pm$ being hypergeometric functions, have frequencies $\omega_L = -\beta^2 \pm \sqrt{\Omega^2 + k^2(2nr - r^2)}$, $r \in \{1, \ldots, n-1\}$. Compared to 1D the frequencies are shifted by β^2 and hence lie in $(-\kappa_\infty - \beta^2, \kappa_\infty - \beta^2)$. The 2D gap solitons propagating in the z-direction have frequencies in $(-\kappa_\infty, \kappa_\infty)$ and hence for $\beta^2 > \kappa_\infty$ there is no overlap of the two frequency regions. This is in contrast with 1D [1] where the two regions are identical.

We note that the above $2n - 1$ linear defect modes are not necessarily the only ones for the defects in question. There may be other stationary solutions whose spatial profile cannot be written as a product $F_\pm(z)G(x)$. These can be, in principle, found numerically as bound state eigenfunctions of (17).

4.2. Nonlinear defect modes

The linear defect modes in Section 4.1 are used as starting points in the construction of nonlinear defect modes. We construct nonlinear defect modes of small total power by regular perturbation methods and modes with larger power numerically via Newton's iteration.

4.2.1. *Nonlinear defect modes with small total power-perturbative construction.* We carry out the perturbation analysis analogously to [1]. With the ansatz $\vec{E}(x, z, t) = e^{-i\omega t}\vec{\mathcal{E}}(x, z)$ the governing system reads

$$\left[\omega + i\sigma_3\partial_z + \partial_x^2 + \sigma_1\kappa(z) + V_1(x) + V_2(z)\right]\vec{\mathcal{E}} + N(\vec{\mathcal{E}}, \vec{\mathcal{E}}^*)\vec{\mathcal{E}} = 0. \quad (21)$$

Let $\omega = \omega_L + \omega^{(1)}|\alpha|^2 + \mathcal{O}(|\alpha|^4)$, $\vec{\mathcal{E}}(x, z) = \alpha[\vec{\mathcal{E}}_0(x, z) + |\alpha|^2\vec{\mathcal{E}}_1(x, z) + \mathcal{O}(|\alpha|^4)]$, where $\vec{\mathcal{E}}_0$ is a linear defect mode with frequency ω_L (see Section 4.1) and $\alpha \in \mathbb{C}$ is a small (in absolute value) parameter. At $\mathcal{O}(|\alpha|)$, we recover the linear equation $\mathcal{L}_0\vec{\mathcal{E}}_0 = 0$ with $\mathcal{L}_0 = \omega_L + i\sigma_3\partial_z + \partial_x^2 + \sigma_1\kappa(z) + V_1(x) + V_2(z)$. At $\mathcal{O}(|\alpha|^3)$, we get

$$\mathcal{L}_0\vec{\mathcal{E}}_1 = -\omega^{(1)}\vec{\mathcal{E}}_0 - N(\vec{\mathcal{E}}_0, \vec{\mathcal{E}}_0^*)\vec{\mathcal{E}}_0,$$

which has an (x, z)-localized solution $\vec{\mathcal{E}}_1$ only if the orthogonality condition $\langle\vec{\mathcal{E}}_0, \omega^{(1)}\vec{\mathcal{E}}_0 + N(\vec{\mathcal{E}}_0, \vec{\mathcal{E}}_0^*)\vec{\mathcal{E}}_0\rangle = 0$ is satisfied. This yields

$$\omega^{(1)} = -\frac{\langle \vec{\mathcal{E}}_0, N(\vec{\mathcal{E}}_0, \vec{\mathcal{E}}_0^*)\vec{\mathcal{E}}_0 \rangle}{\langle \vec{\mathcal{E}}_0, \vec{\mathcal{E}}_0 \rangle}, \tag{22}$$

where the inner product is $\langle \vec{F}, \vec{G} \rangle := \int_{\mathbb{R}^2} F_1 G_1 + F_2 G_2 \, dx \, dz$. Clearly, $\omega^{(1)} < 0$ and the frequency of the nonlinear defect modes bifurcates to the left of ω_L. For the case $n = 1$ in (20) the integrals in (22) can be easily calculated. With $\vec{\mathcal{E}}_0$ normalized so that $\|\vec{\mathcal{E}}_0\|_2^2 = \langle \vec{\mathcal{E}}_0, \vec{\mathcal{E}}_0^* \rangle = 1$ we get $\omega^{(1)} = -\frac{\beta k}{6}$.

In conclusion, consider the defect $V_1(x) = 2\beta^2 \text{sech}^2(\beta x)$ and $V_2(z)$, $\kappa(z)$ as in (5) with $n = 1$. Then, given $\alpha \in \mathbb{C}$ with $|\alpha| \ll 1$, a linear defect mode $\alpha \vec{\mathcal{E}}_0$ with total power $\mathcal{N} = |\alpha|^2$ and frequency ω_L bifurcates into a nonlinear defect mode of total power $\mathcal{O}(|\alpha|^2)$ and frequency $\omega = \omega_L - \frac{\beta k}{6}|\alpha|^2 + \mathcal{O}(|\alpha|^4)$.

4.2.2. Nonlinear defect modes with $\mathcal{O}(1)$ total power–numerical construction.
Once again, we employ Newton's iteration for the construction of "large" nonlinear defect modes. Using a known linear defect mode with $\omega = \omega_L$ and $\mathcal{N} = |\alpha^2| \ll 1$ as the initial guess, we find the nonlinear defect mode with $\omega = \omega_L - \frac{\beta k}{6}|\alpha|^2$ by fixing ω in (21) to this value and solving the system via Newton's iteration with the banded linear solver DGBSV of LAPACK at each step. The resulting mode has $\mathcal{N} = \nu_1 \approx |\alpha|^2$. For a nonlinear defect mode with $\omega = \omega_L - m\frac{\beta k}{6}|\alpha|^2$, we scale the mode with $\omega = \omega_L - (m-1)\frac{\beta k}{6}|\alpha|^2$ to $\mathcal{N} = \nu_{m-1} + |\alpha|^2$ and use it as the initial guess. The result of such a construction can be plotted in a bifurcation diagram for $\mathcal{N}(\omega)$ starting at $\mathcal{N}(\omega_L) = |\alpha|^2$; Figure 8a shows an agreement between the asymptotic approximation (22) and
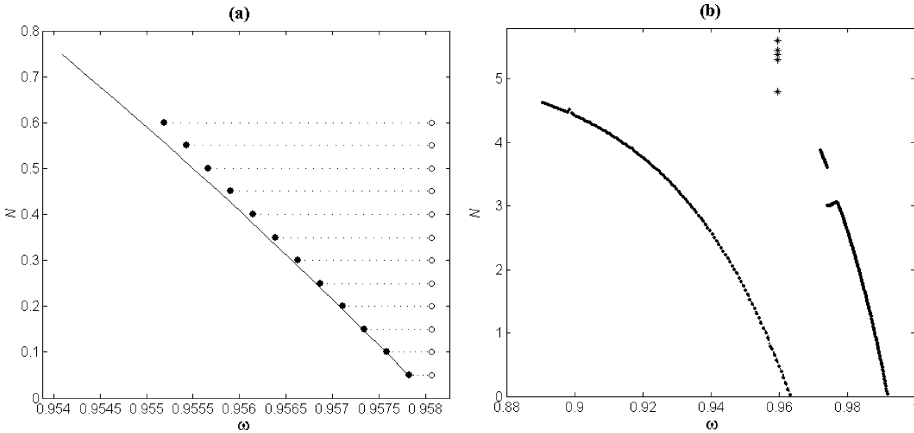
Figure 8.   (a) Bifurcation curve of nonlinear defect modes corresponding to the defect $(\kappa_\infty, n, \beta, k) = (1, 1, 0.16, 0.18)$, $\Omega = \sqrt{\kappa_\infty^2 - k^2}$ (no support truncation)—detail at small $\mathcal{N}$: (-) numerical result, (○) linear defect modes, (●) nonlinear defect modes predicted by the perturbation technique; (b) nonlinear defect modes corresponding to the defect used in Section 4.3.1 ($\omega_L \approx 0.963, 0.992$): bifurcation curves until convergence failure at $\omega \approx 0.8908$, 0.9723, respectively. Stars represent the 5 gap solitons used in Section 4.3.1

the numerical result for small $\mathcal{N}$. The chosen defect belongs to the family (5) and (19) (without any support truncation), for which exact linear defect modes are known. The parameters are $\kappa_\infty = 1$, $(n, \beta, k) = (1, 0.16, 0.18)$, and $\Omega = \sqrt{\kappa_\infty^2 - k^2}$.[2] As expected, with increasing $\mathcal{N}$ the asymptotic form is no longer a good approximation. Figure 8b shows bifurcation curves for two numerically found linear defect modes corresponding to the same defect as used in Figure 8a only with a truncated support. The curves could not be continued due to a failure of Newton's iteration to converge. Similar to the 1D study in [1], we predict trapping if the stationary gap soliton corresponding to the incident gap soliton lies *above* the bifurcation curve of a defect mode. This will ensure both resonance and energetic accessibility.

4.3. Numerical simulations of soliton-defect interactions

In this section we present preliminary results on the interactions of the 2D gap solitons of Section 3.3 with localized defects of the type described in Section 4.1. We wish to verify validity of the mechanism of resonant energy transfer mentioned in Section 2.3 and used to explain trapping of 1D gap solitons in [1]. Compared to the 1D model of [1] there are two major limitations of the so far outlined 2D model. Firstly, gap solitons have been found only for a small range of frequencies within the gap (Section 3.3) and secondly, exact linear defect modes are available only for a class of defects represented as a sum of a truncated x-dependent and a truncated z-dependent potential (Figure 7), which makes finding all the linear defect modes analytically impossible. Other linear defect modes than the family given in Section 4.1 exist and have to be found numerically. This can lead to the existence of many nonlinear defect modes (with different frequencies) into which gap solitons' energy can be transferred. With this in mind the results below still demonstrate the possibility of trapping for the studied defects but a more complete study involving computation of the full set of linear defect modes and their corresponding nonlinear ones as well as determining the relevant frequency definition for the resonance condition is needed to be able to better explain the dynamics.

4.3.1. *Velocity threshold for trapping; wide defect.* In the following numerical experiment, we have $\kappa_\infty = 1$ and use travelling gap solitons with $v = 0.04$, 0.2, 0.3, 0.4, 0.5 corresponding to the stationary gap soliton with $\omega_0 \approx 0.9595$, incident on a relatively wide defect $(n, k, \beta) = (1, 0.18, 0.16)$, $\Omega = \sqrt{\kappa_\infty^2 - k^2}$ (see Section 2.3, 4.1). The support of $V_1(x)$ was truncated via multiplication of V_1 by $0.5 \times (\tanh(z + 9) - \tanh(z - 9))$; similarly, $V_2(z)$ and the variation $\kappa(z)$ away from κ_∞ were multiplied by $0.5 \times (\tanh(x + 7) - \tanh(x - 7))$.

---

[2]For κ_∞, n, and k fixed, Ω is given by studying $\kappa(z)$, i.e., Equation (5) at $|z| \to \infty$. This gives $\Omega = \pm\sqrt{\kappa_\infty^2 - k^2}$. Here, we choose $\Omega > 0$ corresponding to an attractive potential.
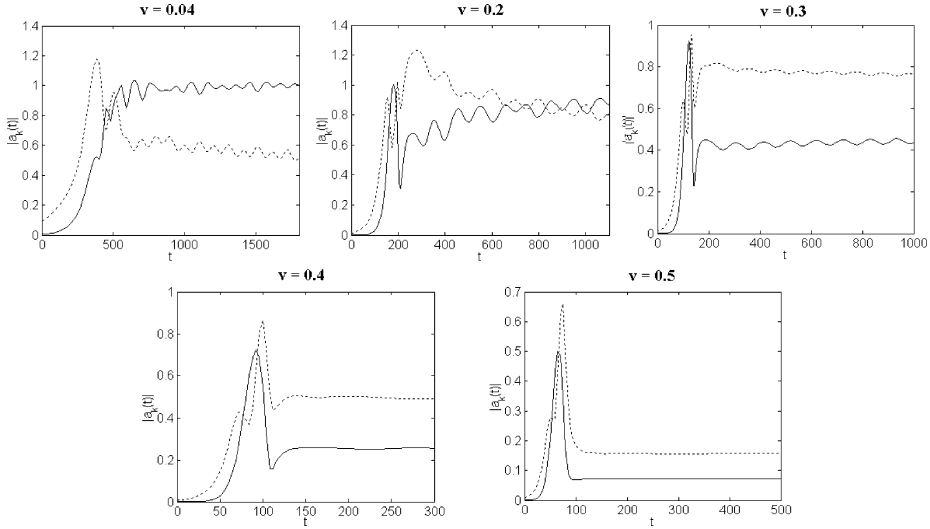
Figure 9. Orthogonal projections of the solutions in Section 4.3.1 onto two corresponding linear defect modes found numerically. The absolute value of the projection coefficients $|a_k(t)|$, $k = 1, 2$ is plotted. Full line: $\omega_L \approx 0.963$, dotted line: $\omega_L \approx 0.992$.

This results in a perturbation of the linear defect mode (and its frequency ω_L) predicted by (4.1). The modes of this 'truncated' defect are found numerically. They have frequencies $\omega_{L_1} \approx 0.963$, $\omega_{L_2} \approx 0.992$. The bifurcation curves of the corresponding nonlinear defect modes are shown in Figure 8b. The gap solitons corresponding to this experiment are represented by the asterisks. Although the bifurcation curves could not be continued numerically further, Figure 8b suggests that the gap soliton lies above the curve corresponding to ω_{L_1} and, if the bifurcation curve corresponding to $\omega_{L_2} \approx 0.992$ exists for ω below 0.9595, then, most likely, also above the other curve. Projection of the trapped solution onto the two linear modes reveals that both modes are activated (Figure 9). Figure 10 reveals that there is a critical velocity[3] $v_c \approx 0.5$ above which virtually no energy is trapped and below which as much as 30% is trapped.

As can be seen from the velocity and amplitude plots, the soliton's first response to the defect is to speed up while first slightly decreasing in amplitude and then focusing. If trapped, focusing and spreading are repeated. These effects are reminiscent of a particle behavior in a potential well but can be better explained as a lens effect of the attractive potential. Also notice that any energy that is transmitted or reflected finally diffracts. This is, again, in contrast with the 1D results of [1], where a 1D gap soliton forms after

---

[3]The velocity is determined from measuring the position of the solution's peak amplitude within the spatial domain.
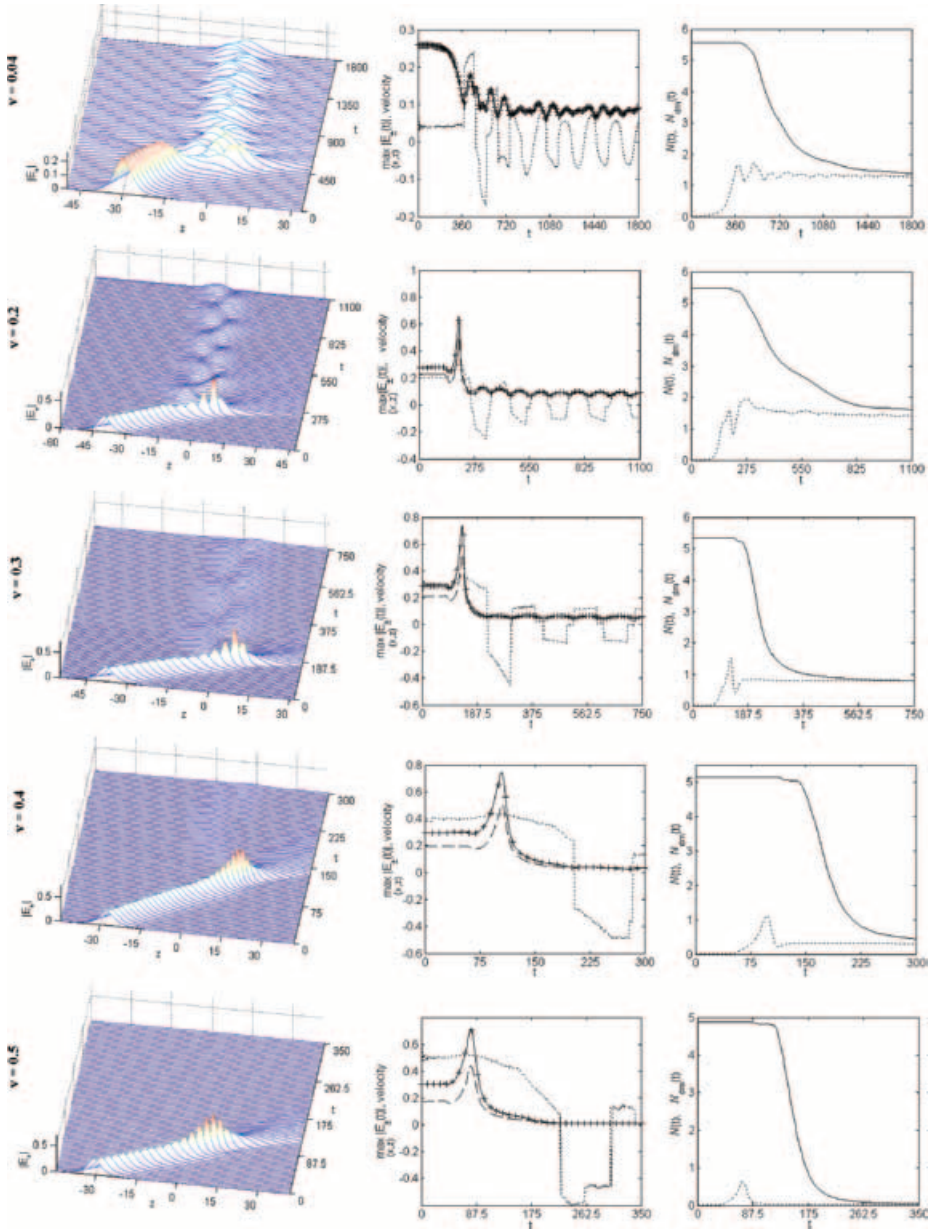
Figure 10. Soliton-defect interaction of Section 4.3.1 for various velocities of the soliton with $\omega_0 \approx 0.9595$ (each row different velocity). Left plot: $|E_+(L_x/2, z, t)|$ ($|E_-|$ is qualitatively the same). Middle plot: (+) $\max_{(x,z)}|E_+|$, (-) $\max_{(x,z)}|E_-|$, ($\cdot$) speed in the z-direction. Right plot: dashed line: total power $\mathcal{N}$, dotted line: power contained in the two linear defect modes.
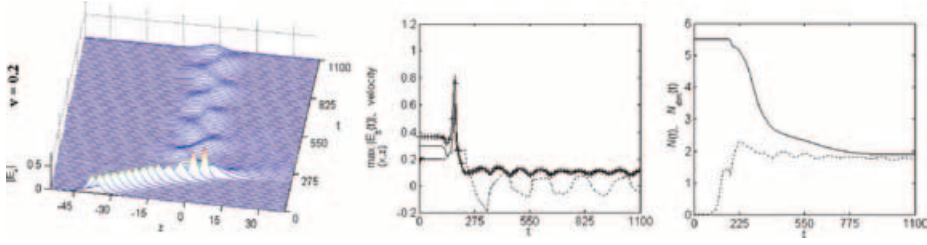
Figure 11. Gap soliton with $\omega_0 \approx 0.929$ and $v = 0.2$ incident on the same defect as in Figure 10. Legend as in Figure 10.

transmission/reflection. We expect this behavior in 2D to be caused by a weaker stability of the 2D gap solitons compared to 1D gap solitons.

For comparison, in Figures 11 and 12 we show gap solitons with $\omega_0 \approx 0.92$, $v = 0.2$, and $\omega_0 \approx 0.9$, $v = 0.04$, respectively, incident on the same defect, i.e., $(n, k, \beta, \kappa_\infty, \Omega) = (1, 0.18, 0.16, 1, 0.9837)$. Because in the $(\omega, \mathcal{N})$-plane the gap solitons lie to the left of those in Figure 10 and closer to the line of nonlinear defect modes, more energy should be trapped. This is, indeed, the case and in Figure 12 about 57% of the energy is trapped.

4.3.2. *x-narrow defect, reflection.* In this simulation, we choose a slow gap soliton obtained not via Newton's iteration but by simply perturbing the ratio of the amplitudes $|\mathcal{E}_+|$ and $|\mathcal{E}_-|$ of the stationary gap soliton with $\omega_0 \approx 0.9595$. Interestingly, this perturbation induces movement though the resulting pulse is a breather. The defect in this simulation is $(n, k, \beta, \kappa_\infty) = (1, 0.18, 0.6, 1)$, $\Omega = -\sqrt{\kappa_\infty^2 - k^2} \approx -0.9837$. Clearly, in this case the family of nonlinear defect modes bifurcating from the one analytically known linear mode (with frequency $\omega_L = \Omega - \beta^2$) should not be resonant with the gap soliton as ω_L is far to the left of ω_0. Figure 13 shows that most of
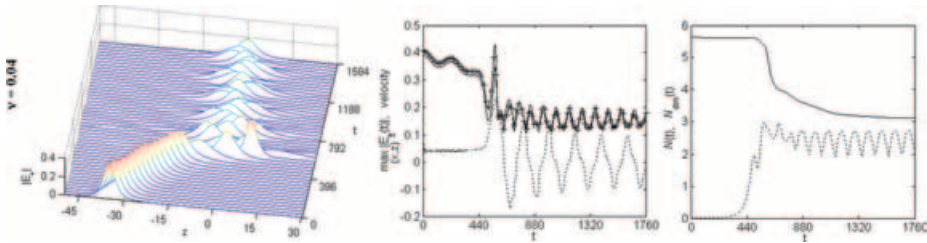
Figure 12. Gap soliton with $\omega_0 \approx 0.9$ and $v = 0.04$ incident on the same defect as in Figure 10. Legend as in Figure 10. The power contained in the linear defect modes is smaller than the total power and hence another defect mode (not found in our numerics) must exist and be accessed.
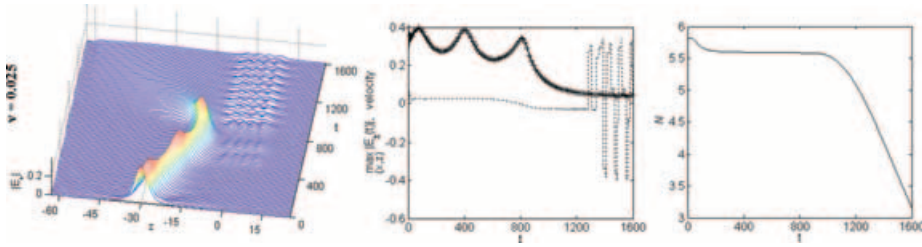
Figure 13.   Soliton-defect interaction of Section 4.3.2. Legend as in Figure 10.

the energy is reflected but, once again, eventually diffracts. We believe that slow moving solitons far from resonance will always mostly reflect.

5. Summary

We demonstrate the existence of both stationary and travelling solitary wave solutions (2D gap solitons) of the 2D CME describing light propagation in Kerr nonlinear 2D waveguides with a Bragg resonant periodic structure in the propagation direction. This is despite the nonexistence of local constrained minima of the corresponding Hamiltonian functional. The travelling gap solitons propagate at any speed less than the absolute value of the group velocity. Evolution of the constructed solutions is checked numerically via a finite-difference time domain code with an ESDIRK-type integration scheme. The successfully constructed solutions occupy a region near the upper edge (from the inside) of the linear frequency gap. Our travelling solitons are the first reported moving localized solutions of 2D CME.

In the second part we present preliminary results on trapping of the above mentioned solitons at localized defects. For selected defect potentials, a family of exact linear defect modes is presented (using results of [1]) and corresponding nonlinear defect modes are constructed numerically. A more complete analysis using other localized defects and identifying their defect modes is necessary to verify the trapping dynamics via a resonant energy transfer between solitons and defect modes. The presented numerical simulations demonstrate the possibility of trapping of slow enough solitons. In these simulations, we take advantage of a perfectly matched boundary layer (PML) treatment of the outgoing radiation.

Acknowledgments

assistance with the numerical parts of their research as well as Roy Goodman (New Jersey Institute of Technology) and Stefano Trillo (University of Ferrara) for valuable comments and discussions.

Appendix: Note on the numerical method for integrating 2D CME

The numerical results of PDE evolution presented in this paper were obtained using a finite difference time-domain method. More concretely, we use 4-th order central difference formulas to approximate the spatial derivatives $\partial_z E_\pm$ and $\partial_x^2 E_\pm$ and a 4-th order explicit/implicit (ESDIRK) Runge–Kutta time integration method [20] to advance the data in time. This time integration method was designed for advection-diffusion equations but serves well in our setting as it allows us to treat the highest order derivative (stiff) terms $\partial_x^2 E_\pm$ implicitly and the remaining terms explicitly, thus requiring a reasonable CFL condition $dt < cdz$. As common for nonlinear advection-type equations without any dissipation, we find it necessary to artificially damp the highest oscillations in the advection direction (z). The usual approach of adding a diffusion term is impractical on long evolution times as the solitary wave structure is lost. Hence, we choose to use a (more expensive) Fourier filter in the z-coordinate to selectively kill only the highest Fourier modes.

An effective treatment of the outgoing radiation is crucial in our simulations where long evolution times on finite domains are required. We use the method of PML [21]; in this approach, the domain is extended beyond the physical boundary by artificial layers (Figure 14) in which the solution is absorbed while ensuring that the interface between the physical domain and the boundary layer is reflectionless. This is done by requiring that the eigenfunctions (in Laplace transform sense) in the layers are identical to those in the physical
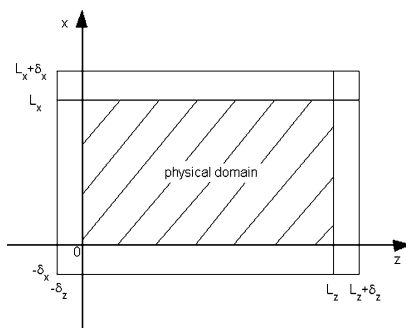
Figure 14. The physical domain and the PML layers.

domain while the eigenvalues change to provide for damping. With our PML formulation the linear system becomes

$$i(\partial_t E_+ + \partial_z E_+ + F_+) + \kappa E_- + \frac{1}{1 + \tilde{\sigma}_x e^{i\rho}} \partial_x \left(\frac{1}{1 + \tilde{\sigma}_x e^{i\rho}} \partial_x E_+ \right) = 0$$

$$i(\partial_t F_+ + \tilde{\sigma}_z \partial_z E_+ + (\alpha + \tilde{\sigma}_z) F_+) + \frac{1}{1 + \tilde{\sigma}_x e^{i\rho}} \partial_x \left(\frac{1}{1 + \tilde{\sigma}_x e^{i\rho}} \partial_x F_+ \right) = 0$$

$$i(\partial_t E_- - \partial_z E_- + F_-) + \kappa E_+ + \frac{1}{1 + \tilde{\sigma}_x e^{i\rho}} \partial_x \left(\frac{1}{1 + \tilde{\sigma}_x e^{i\rho}} \partial_x E_- \right) = 0$$

$$i(\partial_t F_- - \tilde{\sigma}_z \partial_z E_- + (\alpha + \tilde{\sigma}_z) F_-) + \frac{1}{1 + \tilde{\sigma}_x e^{i\rho}} \partial_x \left(\frac{1}{1 + \tilde{\sigma}_x e^{i\rho}} \partial_x F_- \right) = 0,$$

$$(A.1)$$

where $\alpha > 0$, $\rho \in (0, \pi/2)$, $\tilde{\sigma}_x(x)$ and $\tilde{\sigma}_z(z)$ are smooth functions that vanish inside the physical domain $0 \le x \le L_x$, $0 \le z \le L_z$ but are positive inside the x and z layers, respectively, and $F_\pm$ are auxiliary variables defined only in the z-layers ($z < 0$, $z > L_z$). We find that in our case using layers with about 10–15 computational points across their width is sufficient to ensure absorption and to maintain the accuracy of the integration method.

Because in the nonlinear case only radiation waves are expected to reach the PML layers with the main pulse remaining inside the physical domain, the solution inside the layers behaves linearly; hence, after adding the nonlinear terms to the first and third equation, we use the system (A.1) in the nonlinear case also.

References

1. R. H. GOODMAN, R. E. SLUSHER, and M. I. WEINSTEIN, Stopping light on a defect, *JOSA B* 19:1635–1652 (2002).

2. C. SULEM and P. SULEM, *The Nonlinear Schrödinger Equation: Self-focusing and Wave Collapse*, pp. 93–103, Springer-Verlag, Berlin, 2000.

3. A. B. ACEVES and T. DOHNAL, Stopping and bending light in 2D photonic structures, in *Nonlinear Waves: Classical and Quantum Effects*, (F. K. Abdullaev and V. V. Konotop Eds.), pp. 293–302, Kluwer, Dordrecht, 2004.

4. B. J. EGGLETON, R. E. SLUSHER, C. M. DE STERKE, P. A. KRUG, and J. E. SIPE, Bragg grating solitons, *Phys. Rev. Lett.* 76:1627–1630 (1996).

5. B. J. EGGLETON, C. M. DE STERKE, and R. E. SLUSHER, Nonlinear pulse propagation in Bragg gratings, *JOSA B* 14:2980–2993 (1997).

6. N. G. R. BRODERICK, D. J. RICHARDSON, and M. IBSEN, Nonlinear switching in a 20-cm-long fiber Bragg grating, *Opt. Lett.* 25:536–538 (2000).

7. R. H. GOODMAN, R. E. SLUSHER, M. I. WEINSTEIN, and M. KLAUS, Trapping light with grating defects, in *Proceedings of NSF-CBMS Regional Research Conference: Mathematical Methods in Nonlinear Wave Propagation*, Greensboro, NC, May 2002.

8. R. E. Slusher and B. J. Eggleton, Eds., *Nonlinear Photonic Crystals*, Ch. 8, Springer-Verlag, Berlin, 2003.

9. W. Chen and D. L. Mills, Gap solitons and the nonlinear optical response of superlattices, *Phys. Rev. Lett.* 58:160–163 (1987).

10. A. B. Aceves and S. Wabnitz, Self induced transparency solitons in nonlinear refractive media, *Phys. Lett. A* 141:37–42 (1989).

11. D. N. Christodoulides and R. I. Joseph, Slow Bragg solitons in nonlinear periodic structures, *Phys. Rev. Lett.* 62:1746–1749 (1989).

12. A. de Rossi, C. Conti, and S. Trillo, Stability, multistability, and wobbling of optical gap solitons, *Phys. Rev. Lett.* 81:85–88 (1998).

13. I. V. Barashenkov, D. E. Pelinovsky, and E. V. Zemlyanaya, Vibrations and oscillatory instabilities of gap solitons, *Phys. Rev. Lett.* 80:5117–5120 (1998).

14. A. B. Aceves, B. Constantini, and C. de Angelis, Two-dimensional gap solitons in a nonlinear periodic slab waveguide, *JOSA B* 12:1475–1479 (1995).

15. N. Aközbek and S. John, Optical solitary was in two and three dimensional photonic bandgap structures, *Phys. Rev. E* 57:2287–2319 (1998).

16. A. B. Aceves, G. Fibich, and B. Ilan, Gap-soliton bullets in waveguide gratings, *Phys. D* 189:277–286 (2004).

17. I. V. Barashenkov, Stability properties of solutions to nonlinear models possessing a sign—undefined metric, *Acta Phys. Austriaca* 55:155–165 (1983).

18. A. Quarteroni, R. Sacco, and F. Saleri, Numerical mathematics, in *Texts in Applied Mathematics*, Ch. 8, Springer-Verlag, New York, 2000.

19. Y. Saad, *Iterative Methods for Sparse Linear Systems*, Chpt. 6.5, SIAM, Philadelphia, 2003.

20. C. A. Kennedy and M. H. Carpenter, Additive Runge-Kutta Schemes for Convection-Diffusion-Reaction Equations, *NASA Langley Technical Report Server* (2001).

21. T. Hagstrom, A new construction of perfectly matched layers for hyperbolic systems with applications to the linearized Euler equations, in *Mathematical and Numerical Aspects of Wave Propagation Phenomena*, G. Cohen, E. Heikkola, P. Joly, and P. Neittaanmäki, Eds., pp. 125–129, Springer-Verlag, Berlin, 2003.

University of New Mexico